RHESSI Imaging Spectroscopy of the Large Gamma-Ray Flare of July 23, 2002

Last updated: November 26, 2002

A. Gordon Emslie

Department of Physics, The University of Alabama in Huntsville
Huntsville, AL 35899, USA

emslieg@uah.edu

Eduard P. Kontar

Department of Physics & Astronomy
The University, Glasgow G12 8QQ, UK

eduard@astro.gla.ac.uk

and

Sam Krucker, Robert P. Lin

Space Science Lab, University of California
Berkeley, USA

krucker@ssl.berkeley.edu, rlin@ssl.berkeley.edu

ABSTRACT

In this Letter we study spatially resolved hard X-ray spectra of the large X-class flare of July 23, 2002, using data from the RHESSI satellite. Back projection, CLEAN, and forward-fitting algorithms were all employed to produce images in different energy bands. Evaluation of the flux in each energy channel for the prominent features evident in these images allows spectra to be constructed for these features. We find four main features in the flare – a bright, low-energy (soft spectrum) source high in the corona, two localized high-energy (hard spectrum) footpoints and a bright feature bounded by the other three, which we tentatively interpret as a source at the top of a magnetic loop connecting the two footpoints. The temporal evolution of the spectrum of each feature is described, with allowances for the dynamic range of the RHESSI instrument, which obscures weak sources at a certain photon energy when a much brighter source at this photon energy is also present. A comparison with the spatially-integrated spectral evolution of the source is also provided.

Subject headings: Sun: flares

1. Introduction

In this *Letter*, we discuss imaging spectroscopy of the July 23, 2002 flare over the period of main hard X-ray emission, namely from $\sim$ 00:26:00 UT through 00:40:00 UT. During this period, the bulk of the gamma-ray emission from this event also occurred (see Share et al. 2003, this volume), consistent with the acceleration, and precipitation into the dense chromosphere, of MeV-energy protons at the time of observation. Analysis of the hard X-ray emission during this period provides concomitant information on the electron acceleration and propagation processes and hence on the role of electrons vs. protons in the flare impulsive phase.

Here we restrict our discussion to a description of the form of the hard X-ray spectrum in each of four long-lived prominent features within the flare. In §2, we discuss the general source morphology and evolution. In §3 we discuss variations of the hard X-ray spectra with respect to both spatial location and time. In §4, we discuss the results obtained and suggest promising areas for future study.

2. Overall Structure of the Flare and Imaging Algorithms Used

The July 23 flare occurred on the southeast of the solar disk, with the centroid of the soft X-ray emission at approximate coordinates (-890, -240) (arc seconds relative to the solar center). Figure 1 shows images of the event in three energy bands (10 - 15 keV, 35 - 40 keV and 70 - 75 keV, respectively) for three 20-second time intervals (00:26:40-00:27:00, 00:30:00-00:30:20, and 00:33:20-00:33:40 UT) throughout the main phase of the flare. These images were obtained using the CLEAN imaging algorithm.

The emission at low energies ($<\sim$ 30 keV) is dominated by a source with a centroid around (-888,-233); at higher energies three other features become evident. There are two conspicuous bright sources, one centered around (-866,-224) (which we term the "northern footpoint") and one centered around (-870,242) (which we term the "southern footpoint"). In addition, there is a strong suggestion of a bright feature located around (-875,-230), which is most conspicuous in the middle energy ranges (see the 35 - 40 keV frames in Figure 1). Based on the location of this feature relative to the footpoints, and the extended emission connecting the footpoints through this fourth source, we have tentatively labeled this source a "loop-top" source (cf., Masuda et al. 199?). Contours showing the general location of

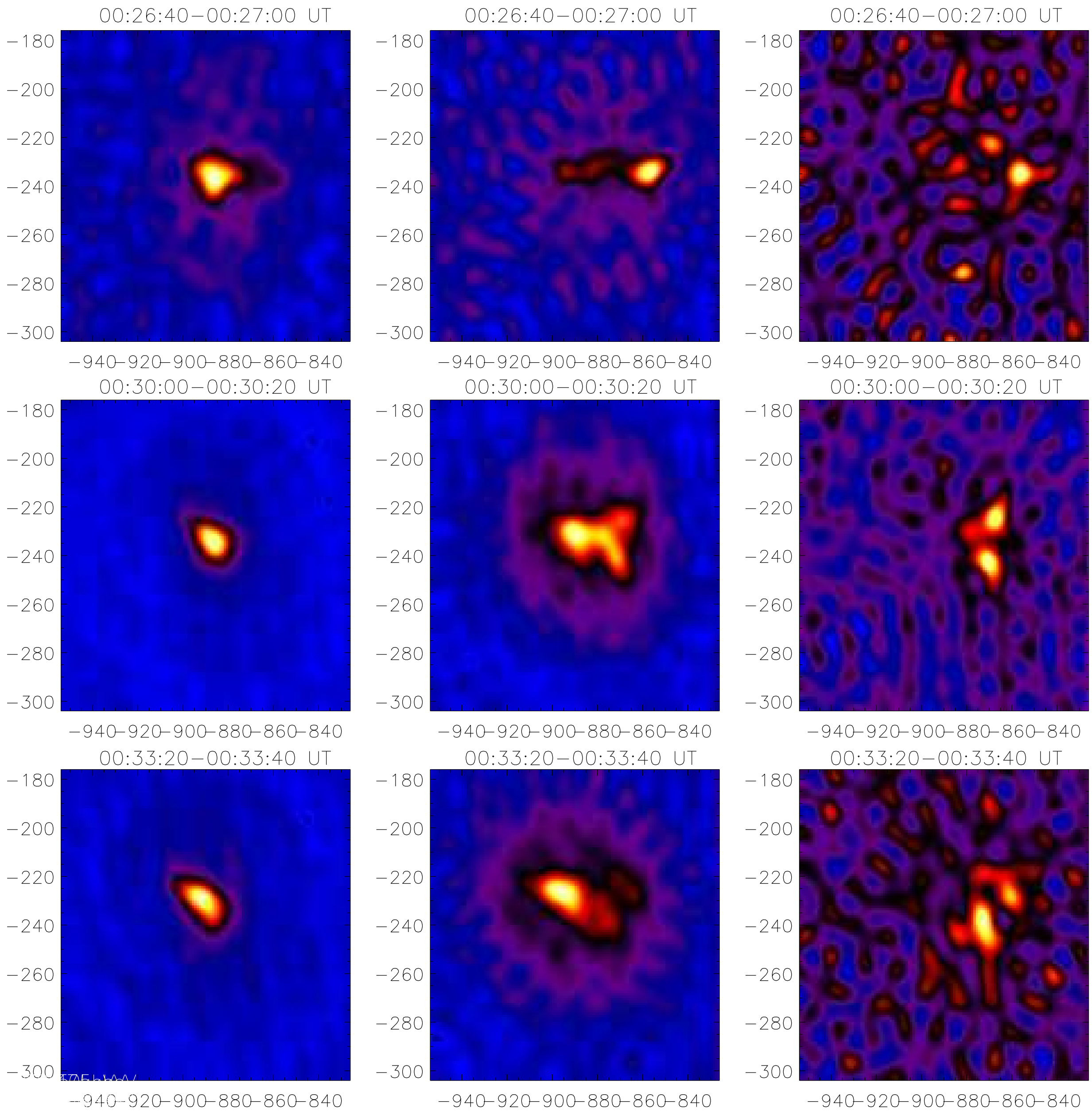

Fig. 1.— CLEAN images for three different time intervals (rows) in the three energy bands 10-25 keV, 35-40 keV, and 70-75 keV (columns).

these features in the source volume are shown in Figure 2.

It should be noted that the spatial structure of the flare region changes on time scales of order minutes, so that the position of the selected features (given above for the time of maximum emission around 00:30:00 UT) does not correspond to the position of these sources at all times. Whether or not the motion of the sources is real or not is a perplexing question. Two of the sources (the "northern footpoint" and the "coronal" source) apparently move to the Northeast (top left of frame) at a rate of approximately 2 arc seconds per minute. This direction is approximately azimuthal (i.e., clockwise around the spacecraft rotation axis) at this solar location. During the flare, there was a failure of the RHESSI roll-determining instrumentation, with the result that the instrument roll angle had to be estimated by interpolation from other times. An error in the roll angle of the spacecraft would have little effect on the morphology of the sources, but could induce an apparent azimuthal motion of the sources over time, consistent with that observed in these two features. However, neither the "southern footpoint" nor the "loop-top" source shows any significant azimuthal motion, implying that roll-solution error cannot be the sole source of the apparent motion of the other two features. A more complete study of source motion in the flare must await a better roll solution for the observing period.

We have chosen to accumulate photons in 18 5-keV energy bands spanning the range from 10 - 100 keV, and into 20-second time intervals spanning the interval from 00:26:20 UT through 00:39:40 UT. (Times both before and after this interval were avoided because of movements of an attenuating shutter around 00:26:10 UT and 00:39:50 UT; both images and spectra obtained over time intervals which include such shutter movements are unreliable.) Since the flux of photons is gradually changing with time, the importance of count statistics, and hence the quality of the images obtained, is variable throughout the event. The most reliable CLEANed images were obtained near the maximum of the flare, i.e. over the period 00:28:40-00:31:20 UT.

The resulting 630 (18 energy bands $\times$ 35 time intervals) images were obtained using the RHESSI imaging software available on the Solar Software (SSW) tree. The images were centered on the point (-890,-240) and extended ± 64 arc-seconds in each direction around this point. 1 arc-second pixels were used in the image reconstruction. Detectors 3 through 8 (which effectively image sources with angular extents in the range from ~ 7 arc seconds through ~ 100 arc seconds) were used. We did not use detector 2 (~ 4 arc-second resolution) in the image processing because of the lack of differentiation between front and rear segment counts in this detector. We also did not use detector 1 (~ 2 arc-second resolution) in view of the uncertain source motion discussed above and the resulting blurring of the images on fine spatial scales. Lastly, we did not use detector 9 (~ 180 arc-second resolution) because the

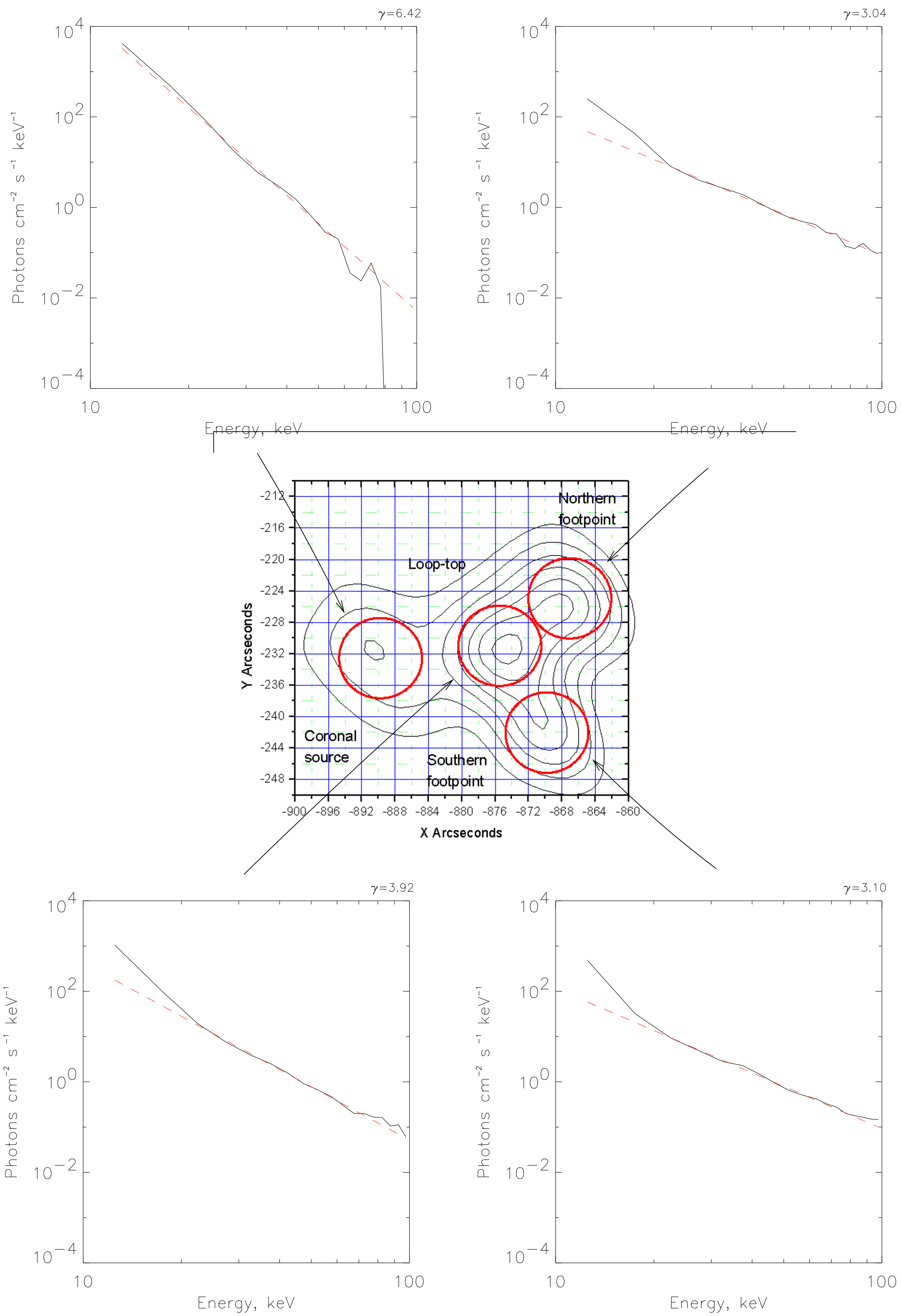

Fig. 2.— Spectra of the four features for the time interval 00:30:00-00:30:20 UT: a) northern footpoint, b) southern footpoint, c) "loop-top" source, d) coronal source. The best-fit power-law spectra, determined by the points in the range 20-60 keV, are also shown.

X-ray features evident all occurred on size-scales significantly less than this. (We note that Share et al. 2003 [this volume] *have*, however, used detector 9 to "image" [or, more accurately, locate] the gamma-ray emission from the event [since the grids in front of detector 9 are the only ones thick enough to modulate gamma-ray radiation]; the position of the gamma-ray emission centroid is consistent with the location of the "footpoint" sources that we discuss in this *Letter*.)

3. Source Features and their Spectra

After producing "quick-look" images with the back-projection method (Schmahl 19??), the images were refined using both the CLEAN and forward-fitting algorithms, using the default parameters appropriate to Release Version 5.0 of the RHESSI software tree. Figure 2 shows the photon spectrum of each of the four prominent features, for the time interval 00:30:00 - 00:30:20 UT. At low energies, the spectra of the footpoint and looptop sources are unreliable. Indeed, Figure 1 shows that throughout the event there is an apparent absence of emission from the footpoints at low energies (and an apparent absence of emission from the coronal source at high energies). This behavior is due to the finite dynamic range ($\sim 10:1$) of the RHESSI instrument: fluxes from sources weaker than ~ 0.1 of the intensity of the brightest source present at that time are not accurately determined by the imaging algorithm. Thus sources with steep spectra dominate the images at low energies, while sources with flat (hard) spectra dominate at high energies. Figure 2 shows that at 10 keV, the coronal source flux is some two orders of magnitude brighter than the footpoint sources, while at 100 keV, it is some two orders of magnitude fainter. Since these ratios exceeds the dynamic range of the RHESSI instrument, imaged fluxes at low (high) energies are not accurately determined for the footpoint (coronal) sources, respectively; meaningful spectra can be obtained only over the spectral range where dynamic range factors are not a consideration, i.e. where the ratio of fluxes in the various features lies within an order of magnitude or so. From Figure 2 we see that the ratio of coronal to footpoint emission varies from 10 to 0.1 over the photon energy range from ~ 20 keV to ~ 60 keV. Reliable spectra for all source features can therefore be determined only over this energy range.

Figure 2 shows fits to the spectra of each of the four source features to power-law forms, using only emission in the reliable energy range from 20 - 60 keV, for a time interval close to the peak emission period, viz. 00:30:00 - 00:30:20 UT. Each fit is labelled with the value of the power-law spectral index $\gamma = -\mathrm{d}\log(I(\epsilon))/\mathrm{d}\log(\epsilon)$ appropriate. The footpoint sources show relatively hard specrl indices of 3.04 and 3.1, respectively, while the coronal source has as spectral index of ~ 7. The spectral index for the "looptop" source is 3.9, approximately one power steeper than the footpoints. The theoretical implications of these spectral index differences will be the subject of a future paper.

4. Time Evolution of the HXR Spectra in Different Features

The morphology of the X-ray emitting region, particularly at higher energies > 30 keV, changes on a timescale of a few minutes. This is exemplified quite clearly in the range $70-75$ keV (see Fig. 1). The two footpoints appear almost simultaneously around 00:28:00 UT, while in the later phases of the flare the emission from the southern footpoint expands along a line of faint emission connecting the two footpoints, presumably a magnetic loop. (An attempt was made to compare the hard X-ray images with images from the TRACE instrument in order to gtry and determine the magnetic connectivity of the features, but unfortunately the TRACE images were saturated with emission during this very intense event, rendering a determination of the loop structure impossible. Examination of Hα images from Big Bear Solar Observatory (?) reveals structures consistent with a magnetic loop connecting the footpoint sources along the line of emission evident in the hard X-ray images – Vilmer 2003). This expansion of the footpoint source with time is exactly what would be expected from considerations of chromospheric evaporation in the heated flare loop (e.g., Mariska, Emslie & Li 1989), in which the chromospheric target is heated and rises up the magentic loop connecting the two footpoints, producing a greater target density, and so an increase in hard X-ray emission, higher in the loop as time progresses.

Figure 3 shows the behavior of the best-fit power law spectral index $\gamma = -\mathrm{d}\log(I(\epsilon))/\mathrm{d}\log(\epsilon)$ (obtained by fitting the spectrum over the range from $20-60$ keV) for each of the four features over the duration of the main phase of the flare. (The spectral indices for the footpoint and looptop sources are unreliable at the beginning of the event, because of the dynamic range issues discussed above.) During the period from 00:30 UT to 00:34 UT, the spectrum of both the footpoint and looptop sources shows a gradual softening (by approximately one power) with time; there is a subsequent, more sudden, hardening of the footpoint sources from 00:34 UT to 00:35 UT. On the other hand, the coronal source show a relatively constant spectral index $\gamma \approx 6.5$ throughout the event. Holman et al. (2003; this volume) have derived fits to the *spatially integrated* hard X-ray emission for the event. These spectra are determined rather straightforwardly from detector counts in each energy channel and are not subject to the dynamic range limitations of imaged spectra. Holman et al. find that the spectrum at lower energies is characterized by an excess of emission over the power-law fit ($\gamma \simeq 3$) that characterizes the emission at energies above ~ 30 keV, which they interpret as thermal emission with a temperature of order 50 million K. Particularly in view of the fact that a power-law source can be produced in a relatively straightforward manner by a thermal source (with a power-law distribution of differential emission measure – Brown 1975; Brown & Emslie 1988), our results are not inconsistent with such a thermal interpretation of the coronal source.

Superimposed on the plots for the footpoint and coronal sources is the variation of γ for the spatially-integrated emission outside of the thermally-dominated region (Holman et al. 2003; this volume). We see that the spectral evolution of the of the footpoints closely follows the temporal evolution of spatially integrated spectra (Holman et al, *this issue*).

In summary, we find that the emission at low energies is dominated by the coronal feature, the spectrum of which is steep and consistent with a thermal source. At higher energies, the harder footpoint and looptop features dominate the emission. Indeed, the variation with time of the spectral indices of the footpoint features nicely matches the variation in the spectral index for the emission for the flare as a whole. This observation validates the spectral indices determined through the "comparison-of-images-at-different-energies" approach.

5. Summary and Conclusions

First and foremost, we have shown that the RHESSI instrument has fulfilled its promise of producing imaging spectroscopy data of high quality. For the July 23, 2002 event, the emission is concentrated in four features – a coronal source with a steep spectrum, two footpoints with relatively hard spectra, and a "looptop" source with a spectrum intermediate between the other features.

Although space limitations limit a full discussion of the theoretical implications of the data, a few points deserve comment. First, the spectra for the two footpoint sources track each other very well (Figure 3). The spectrum for the "looptop" source tracks the gradual softening evident in the footpoint sources; the spectral index difference between the looptop and the footpoints is of order 1.0. Such a difference is broadly consistent with collisional hardening of the spectrum between the looptop and footpoint sources. Because of the inverse energy dependence of the collisional cross-section, the electron spectrum arriving at the footpoints (and hence the resulting bremsstrahlung spectrum) is hardened relative to that at the "looptop".

In a future paper, we will analyze these variations of spectrum with respect to both space and time, and their implications for models of electron acceleration and propagation in solar flares.

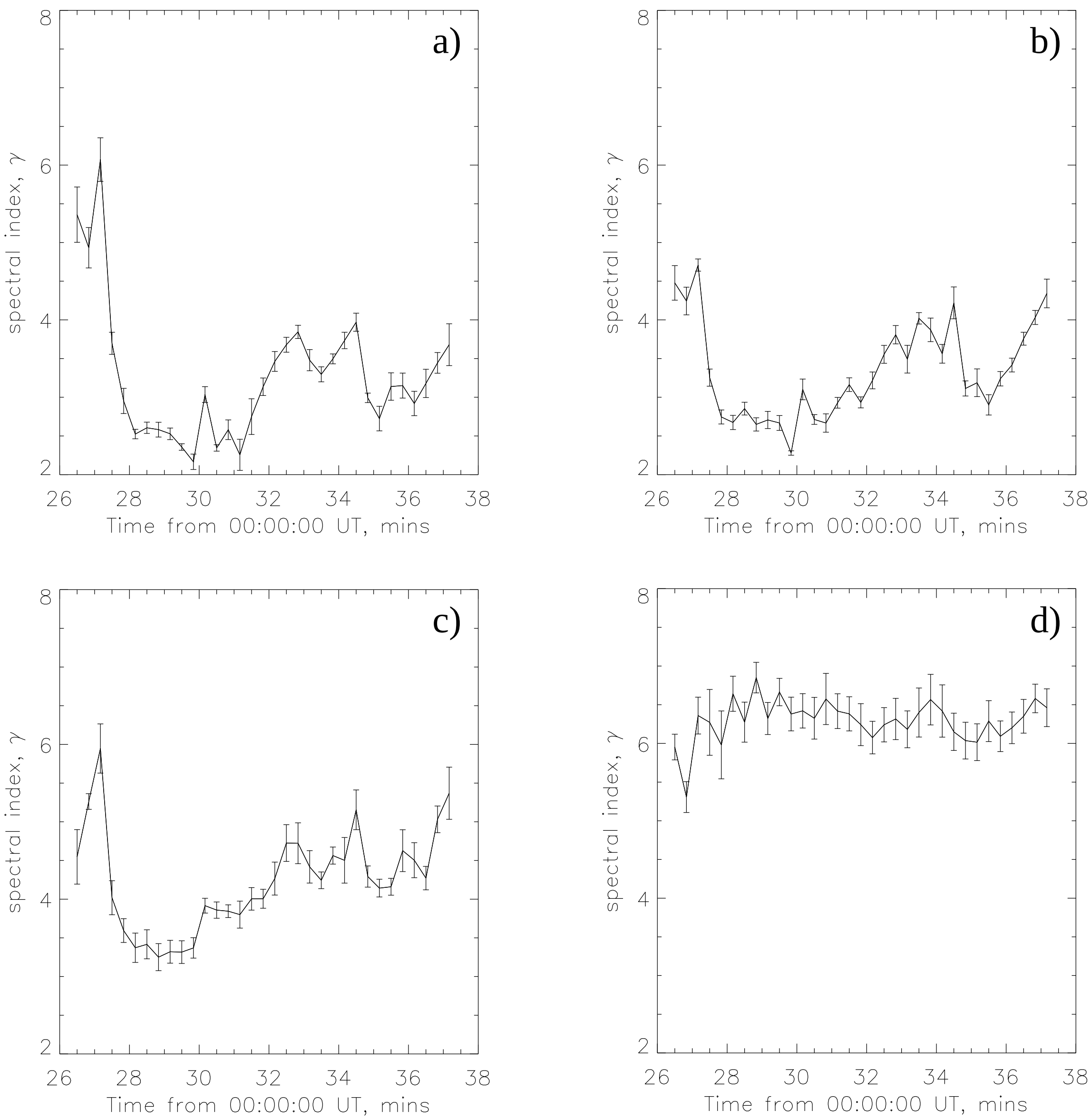

Fig. 3.— Temporal variations of the best-fit spectral index, γ, in the range 20-60 keV, for four selected bright features: a) northern footpoint, b) southern footpoint, c) "loop-top" source, d) coronal source. The inset figures show the relation of the feature to the overall flare emission.

This work was supported by NASA's Office of Space Science and by the UK PPARC.

REFERENCES